Chemosphere 246 (2020) 125763

Contents lists available at ScienceDirect

Chemosphere

journal homepage: www.elsevier.com/locate/chemosphere

Effect of calcination time of a quadruple-element doped titania nanoparticles in the photodegradation of gaseous formaldehyde under blue light irradiation

Maricris T. Laciste [a, b], Mark Daniel G. de Luna [a, c], Nolan C. Tolosa [d], Ming-Chun Lu [e, *]

[a] Environmental Engineering Program, National Graduate School of Engineering, University of the Philippines, Diliman, Quezon City, 1101, Philippines
[b] Environmental Quality Management Division, Environmental Management Bureau, Department of Environment and Natural Resources, Quezon City, 1101, Philippines
[c] Department of Chemical Engineering, University of the Philippines, Diliman, Quezon City, 1101, Philippines
[d] Department of Chemical Engineering, College of Technology, University of San Agustin, Iloilo City, 5000, Philippines
[e] Department of Environmental Resources Management, Chia-Nan University of Pharmacy and Science, Tainan, 71710, Taiwan

HIGHLIGHTS

- Residual formaldehyde meets the standard limit of OSHA PEL, ACGIH C and USGBC LEED.
- C_{y35} photocatalyst classified as Type IV with H2 hysteresis loop according to BDDT.
- Decrease in SSA of C_{y35} catalyst is due to pore blocking and sintering process.

GRAPHICAL ABSTRACT

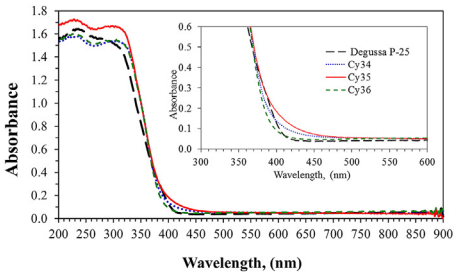

ARTICLE INFO

Article history:
Received 29 August 2019
Received in revised form
6 December 2019
Accepted 25 December 2019
Available online 30 December 2019

Handling Editor: Jun Huang

Keywords:
Calcination duration
Gaseous formaldehyde
Indoor air purification
Visible-light photocatalysis
VOC emissions

ABSTRACT

The photocatalytic degradation of gaseous formaldehyde using Ag/F/N/W-doped titanium dioxide was examined. The photocatalytic reaction was conducted using photocatalysts immobilized on glass tubular reactors illuminated under blue LED lights. Factors affecting gaseous formaldehyde degradation such as photocatalyst's calcination time and dosage, initial formaldehyde concentration, light intensity and operating temperature were studied. Results show that the photocatalytic degradation rate increases with pollutant concentration indicating no mass transfer limitations within the formaldehyde concentration range used. The photodegradation of the formaldehyde using catalyst calcined for 5 h reached ~88%. The photocatalyst concentration giving the highest degradation rate is found to be 0.10 gL^{-1}. Which means that upon increasing the concentration of the immobilized photocatalysts will increase its thickness and it may not increase the number of the photo-induced particles. On the other hand, increasing light intensity and operating temperature increased the photocatalytic degradation of gaseous formaldehyde. The maximum light intensity and operating temperature were measured at 25 Wm^{-2} and 40 °C, respectively. Langmuir-Hinshelwood kinetic type model was used to describe the photocatalytic reaction. The photocatalytic degradation behavior of gaseous formaldehyde on the modified photocatalyst follows a pseudo-first order rate equation based on a Langmuir-Hinshelwood kinetic type model.

* Corresponding author.
E-mail address: mmclu@mail.cnu.edu.tw (M.-C. Lu).

https://doi.org/10.1016/j.chemosphere.2019.125763
0045-6535/

1. Introduction

Indoor air volatile organic compounds (VOCs) with concentration ranging from 500 to 1000 ppb, such as gaseous formaldehyde (CH_2O), are classified into toxic, carcinogenic and persistent gaseous contaminants based on their pollution characteristics Pei et al. (2020); Debono et al. (2013); Liu et al. (2008); Rezaee et al. (2013). Indoor air quality such as the VOCs may reach as high as concentration of 1 mgL^{-1}(ppm) Debono et al. (2013); Cheng et al. (2013); Zhong et al. (2009). At present, because of high standard living, about 80–90% of the time of society remains in closed environment. As such, indoor air quality has an immense impact in individual's health and productivity wherein the infants and elderly are more susceptible characteristics Yu et al. (2009); Lai et al. (2007).

Formaldehyde on the other hand, is one of the main components of various building materials such as particle board, pressed wood, wallpaper, paint, furnishings and other decorating materials, and activities from cooking, use of electric appliances and devices Salthammer (2019); Harb et al., 2020; Xiao et al. (2013); Liu et al. (2008); Sánchez et al. (2012). In several cases, average indoor formaldehyde concentrations exceeded the maximum allowable concentration (0.1 mgm^{-3}) set by the World Health Organization (WHO) and the U.S. Environmental Protection Agency (USEPA) for indoor air quality Salthammer (2019); Xiao et al. (2013). Air pollutant treatment using absorption/adsorption has been already established in controlling indoor air especially in pharmaceutical industries and in electronic control panel systems.

Photocatalysis has been extensively employed in the investigation of gaseous pollutant's decomposition in both indoor and outdoor environments. One of the active catalysts used in titanium dioxide (TiO_2) due to high photocatalytic activity, stability in corrosion, non-toxic and low cost Villaluz et al. (2019); Lin et al. (2016); Tolosa et al. (2011a).

One of the major drawbacks of the commercial TiO_2 photocatalyst application is its ability to utilize the visible light photons Lin et al. (2016); Fujishima et al. (2008); found that bombarding TiO_2 photocatalyst with various transition metal ions in the presence of a strong electric field shifts, enhances the catalyst's absorption band towards the visible light region and magnitude of the shift depends on the type of metal ion (V > Cr > Mn > Fe > Ni) implanted on the catalyst. It was noted that the high band energies of pure TiO_2 in rutile (3.0 eV) and anatase (3.2 eV) phases limit the photo-excitation in the near ultraviolet region ($\lambda < 400$ nm) He et al. (2012); Tabaei et al. (2012).

Research study proved that addition of transition metal ions such as Fe^{3+} Sonowane et al. (2004), Mo^{5+} Haber et al. (2008), $Ru2^{+}$ Senthilnanthan et al. (2012), V^{5+} Wu and Chen (2004) and Cu^{2+} De Luna et al. (2019) improved the photo activity of TiO_2. These metal ions act as electron-hole pair, suppressing the recombination and trapping that widens the available wavelength range, subsequently increasing the utilization rate of visible light Wilke and Breuer (1999); Zhang and Liu (2008).

Tungsten doping on the other hand, is found to have photochromic effects in photocatalysis systems that would be significant in detection of volatile organic compound. The photochromism of tungsten is attributed to the reduction of W^{6+} to W^{5+} during photocatalysis Jin et al. (2011). At the same time, W^{6+} acts as an electron trap which limits the charge recombination of TiO_2 photocatalyst during reaction. It has also the tendency to decrease the density of oxygen vacancy and retard crystal grain growth Wu et al. (2005). Studies in tungsten doping found to have considerably improved the visible-light photo activity of TiO_2. Using sol-gel method and hydrothermal treatment, it was observed that TiO_2 doped with 0.5% W and treated with hydrothermal curing in 4 h showed photo activity under blue light irradiation Putta et al. (2011).

Studies conducted by Wu et al. (2005) presented that in W-doped TiO_2 samples, tungsten has three valences (W^{6+}, W^{5+}, W^{4+}), and titanium has two (Ti^{4+}, Ti^{3+}) Wu et al. (2005). W^{6+} can enter the crystal lattice of titanium dioxide because it has similar radii with Ti^{4+}.

There were already few studies on gaseous formaldehyde removal by visible light photocatalysis using doped-TiO_2 that have been published and this includes N–F–TiO_2 Li et al. (2010), Ni:N–TiO_2 Zhang and Liu (2008). C:N–TiO_2 Han et al. (2013); Wang and Lim (2011).

The kinetic model proposed in photocatalytic degradation of gaseous formaldehyde using titanium dioxide photocatalyst has been described by Langmuir-Hinshelwood (L-H) model Liu et al., 2005; Shie et al. (2008). For a single-site L-H model (i.e., one contaminant system), only gaseous formaldehyde used as the contaminant and the photocatalytic degradation rate is given by Equation (1).

$$r = \frac{dC_t}{dt} = \frac{kKC_t}{1 + KC_t} \tag{1}$$

where r is the reaction rate ($ppmh^{-1}$), t is the illumination time (h), k is the apparent kinetic constant ($ppmh^{-1}$), K is the adsorption equilibrium constant (ppm^{-1}), C_t (ppm) is the contaminant concentration at time t.

If KC_t is much less than 1 and the C_o is small, the first-order oxidation kinetics can be observed and the reaction rate constant denotes as K'. Equation (1) can be written as Equation (2).

$$r = -\frac{dC_t}{dt} = K'C_t \tag{2}$$

where K' is the apparent first-order reaction coefficient (h^{-1}).

Integrating Equation (2), the new form of equation is presented in Equation (3).

$$C_t = C_o e^{-K't} \tag{3}$$

Using logarithmic function, Equation (3) can be linearly expressed as Equation (4).

$$lnC_o - lnC_t = K't \tag{4}$$

Using linearized pseudo-first order plots of $-\ln(C_t/C_o)$ versus time, the apparent rate constant K' can be deduced.

Using the same condition for second-order kinetics of a multiple-site L-H model, the photocatalytic degradation rate is given by Equation (5).

$$r = \frac{dC_t}{dt} = \frac{kKC_t^2}{1 + KC_t^2} \tag{5}$$

If KC_t is much less than 1 and the C_o is small, the second-order oxidation kinetics can also be observed and the reaction rate constant denotes as K". Equation (5) can be simplified as Equation (6)

$$r = -\frac{dC_t}{dt} = K''C_t^2 \tag{6}$$

where K'' is the apparent second-order reaction coefficient ($ppm^{-1}h^{-1}$).

Integrating and using logarithmic function, Equation (6) will have the new simplified form of linear equation expressed as Equation (7).

$$\frac{1}{C_t} - \frac{1}{C_o} = K''t \quad (7)$$

The linearized pseudo-second order plots of $(1/C_t - 1/C_o)$ versus time generates a slope (K").

In this study, we examined the effect of the calcination time applied to synthesized photocatalyst immobilized on the glass tubular reactor on the kinetics of gaseous formaldehyde photocatalytic degradation. Other factors such as the effect of photocatalyst concentration, initial formaldehyde concentration, light intensity and operating temperature were also elucidated.

2. Materials and methods

The synthesized photocatalyst was used to degrade gaseous formaldehyde at varying experimental conditions. All chemicals used in preparation of the synthesized photocatalyst were analytical grade. Photocatalysts were synthesized using a modified sol-gel method conducted by Tolosa et al. (2011b). TiO_2 sol mixture was prepared from 10 mL titanium (IV) butoxide ($C_{16}H_{36}O_4Ti$, 98%, Merck) as precursor, mixed with 40 mL ethanol (C_2H_5OH, 99.5%, Merck) in a flask with constant stirring of 400 rpm using a Corning stirrer hot plate. After 5 min, 10 mL deionized (DI) water with resistivity value of 18.2 MΩ cm was added to the mixture and continuously stirred for 1 h until a homogeneous white sol was formed. Prepared aqueous solution of dopants, ammonium fluoride (NH_4F, 99%, Ferak GMBH), silver nitrate ($AgNO_3$, 99.8%, Ferak GMBH) and sodium tungstate dihydrate ($Na_2WO_4 \cdot 2H_2O$, 99%, Ferak GMBH) was added dropwise in the homogeneous mixture. Another 10 mL of ethanol was added to the mixture followed by stirring until the solution was completely mixed. At this point, the TiO_2 sol was cured for 24 h at an ambient temperature for complete hydrolysis. The precipitated solid samples cured for 24 h were dried in a Shin Shiang Tech RUD-45 L Oven for 24–48 h at 80 °C. The dried solid was size reduced and passed through a sieve with mesh number 230 to even out the size of the dried solid and transferred to a crucible dish for calcination in a Vulcan A-550 Furnace.

The physical and structural properties of the different photocatalyst were examined using a PANalytical XPERT-PRO X-ray Diffraction (XRD) spectrophotometer. Surface properties such as chemical state and ionic state information were determined using ULVAC-PHI 5000 Versa Probe X-ray Photoelectron Spectrometer (XPS) and functional groups were analyzed and evaluated using a JASCO FT-IR 4100 Fourier Transform Infra-red (FTIR) spectrophotometer. Optical properties were analyzed using a Hitachi U–3900H UV–Vis Reflectance Spectrophotometer.

Photocatalytic experiments were conducted in a 20-mL tubular borosilicate glass reactor housed inside a 0.216 m^3 airtight box with temperature controller similar to our previous work Laciste et al. (2017); De Luna et al. (2018). HR 16 blue light emitting diode (LED) (λ ≈ 440–490 nm) was used as the visible light source. Initially formaldehyde concentration was measured at the start of the experiment to establish a baseline prior to destruction. The stock formaldehyde solution was prepared from formaldehyde (CH_2O, 37%, Ferak GMBH). Two microliters of the standard solution are dropped inside the glass tube reactors 12 cm from the bottom of the tubes. The tubes are sealed using a septum made of polytetrafluoroethylene (PTFE) and sealed with parafilm tapes. The tubular reactors were wrapped with aluminum foil to protect against the light degradation. The set-up was heated on a Newlab HP-303D hot plate at a temperature of 40 °C for 1 h to completely vaporize the formaldehyde solution in the system. The system is allowed to stand for 2 h in the dark at a controlled temperature to reach adsorption equilibrium between formaldehyde vapor and photocatalyst. The tubular reactors were then illuminated by the LED bulbs and samples were taken at a 30-min interval (0, 30, 60, 90, 120 min) using Htv Formaldemeter, PPM Technology for direct measurements.

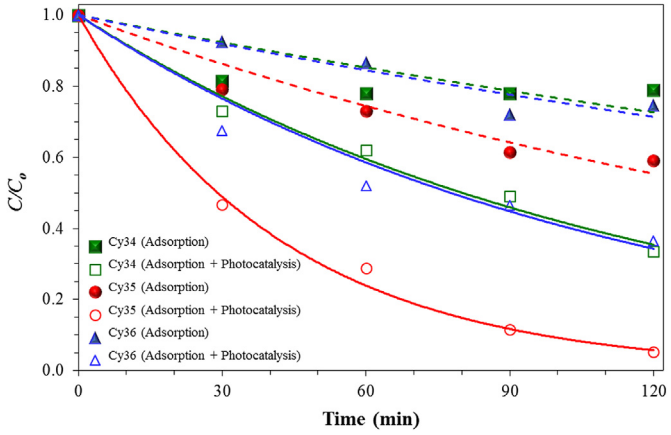

Fig. 1. Residual formaldehyde plot using synthesized photocatalysts calcined at different calcination time. 0.1 gL^{-1} photocatalyst, 4 ppm formaldehyde, 30 °C, Adsorption (0 Wm^{-2}), Photocatalysis (Vertical 10 Wm^{-2}/Horizontal 25 Wm^{-2}).

Adsorption experiments were also conducted in the dark with the similar experimental conditions (*i.e.*, photocatalyst concentration, formaldehyde initial concentration, and temperature) to establish adsorption capacity of photocatalyst that contributes to the degradation reaction.

3. Results and discussion

3.1. Effect of calcination time

Fig. 1 represents the residual formaldehyde plots using doped-TiO_2photocatalysts with varying calcination time (4 h, 5 h, 6 h) which is represented by C_{y34}, C_{y35}, and C_{y36}, respectively. It is remarkable to note that C_{y35} has the highest photocatalytic degradation of gaseous formaldehyde among the photocatalysts, C_{y34} and C_{y36}. The effect of the calcination temperature of the photocatalysts can be correlated in the photocatalytic degradation of gaseous formaldehyde. This can be shown in Fig. 2 of the UV–Vis DRS spectra of modified photocatalysts at different calcination. The spectra show that absorption edge of the C_{y35} with calcination time of 5 h has higher absorption wavelength with lower band gap energy compared with the Degussa P-25, C_{y34}, and C_{y36}. As shown in

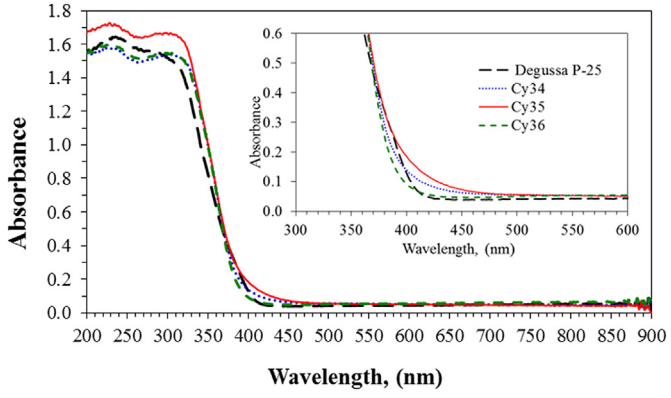

Fig. 2. UV–Vis spectrum of TiO_2 photocatalysts calcined at different calcination time.

Table 1
Calculated band gap energies of Degussa P-25 and the synthesized photocatalysts calcined at different temperatures.

Photocatalyst	Calcination time (h)	Cut off wavelength, λ (nm)	Band gap energy, E (eV)
Degussa P-25	–	412	3.02
Cy34	4	410	3.03
Cy35	5	421	2.95
Cy36	6	405	3.07

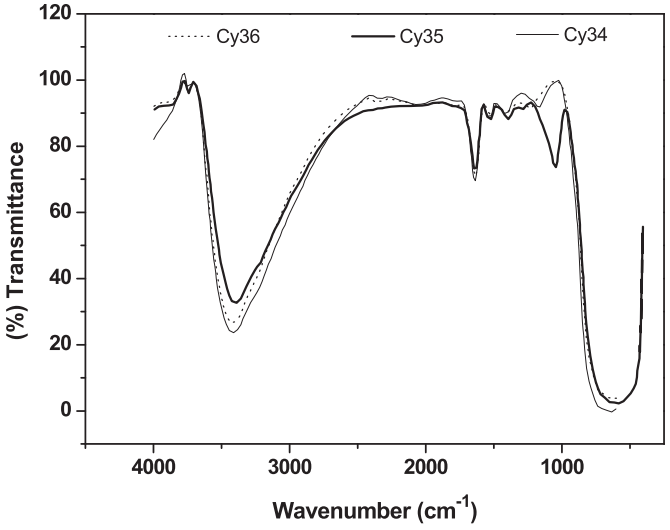

Fig. 3. FTIR spectra of synthesized photocatalysts calcined at varying duration.

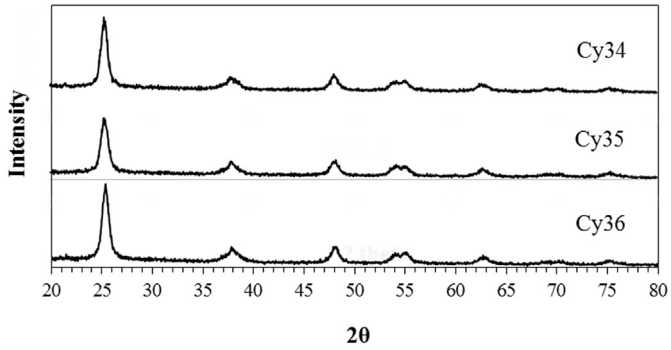

Fig. 4. XRD spectra of synthesized titanium dioxide photocatalyst calcined at 300°C with different calcination time (C_{y34}, C_{y35}, C_{y36}).

Fig. 2 and Table 1, C_{y35} exhibits a cut-off wavelength of 421 nm and displays a better absorption wavelength over Degussa P-25, C_{y34}, and C_{y36} ($\lambda_{Cy36} < \lambda_{Cy34} < \lambda_{Degussa\ P\text{-}25} < \lambda_{Cy35}$). The photocatalyst C_{y35} falls within the spectrum of the blue light which implies a highest possibility on absorbing photons from visible light. The absorption wavelength threshold (λ) can be correlated and significant with the photocatalytic activity of the synthesized photocatalysts. As such, the higher the absorption threshold of photocatalyst, the higher the gaseous formaldehyde's photodegradation.

The FTIR spectra of the synthesized photocatalysts with varying calcination time shows the relative intensities of the OH-stretching are presented in Fig. 3. The movement of the degradation pattern is also significant to the trend in the relative intensities of the OH-stretching (1630–1660 cm^{-1}) of the FTIR results as shown in

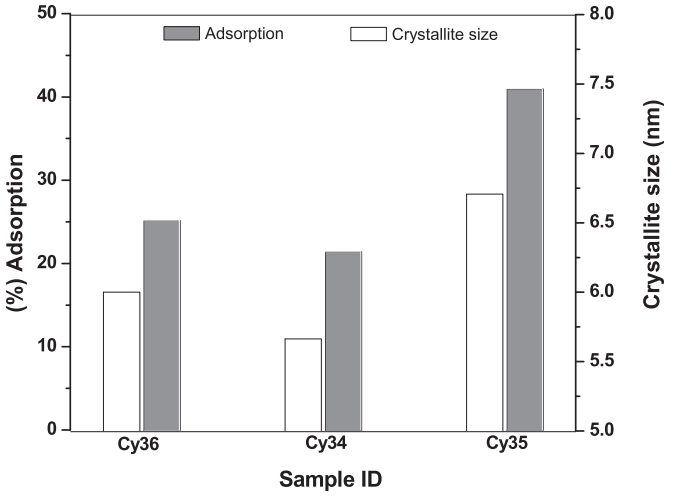

Fig. 5. Adsorption residual formaldehyde concentration after 2 h runtime against crystallite size of photocatalysts calcined at different calcination time.

Fig. 3. This can be attributed to attached water molecule and TiO-stretching (450–620 cm^{-1}) De Luna et al. (2018). The FTIR results suggest that the available hydroxyl groups attached to the surface of the photocatalyst is one of the key players in the photocatalytic reaction of gaseous formaldehyde. Moreover, the trend is also similar to the shift of the same bands of the photocatalysts associated with the OH group. Another relative intensity of the bands assigned with OH-stretching at 3390–3410 cm^{-1} do not associate to the calcination time from which the C_{y35} exhibits the lowest intensity. This verifies the weak absorption of water and shifted towards decreasing wave number ($C_{y34} > C_{y36} > C_{y35}$). The FTIR spectra of C_{y34}, C_{y35}, and C_{y36} photocatalysts show almost similar absorption bands. The bands associated with OH bending (1630–1660 cm^{-1}) shifts towards increasing wave number and the values arranged in increasing order $C_{y34} < C_{y36} < C_{y35}$. Photocatalyst C_{y35} calcined at 300 °C for 5 h showed the greatest shift towards increasing wave numbers.

The XRD spectra of synthesized photocatalysts C_{y34}, C_{y35}, and C_{y36} calcined at 300 °C with calcination time of 4, 5, and 6 h, respectively is shown in Fig. 4. The patterns of the spectra show that the crystal phases for all the synthesized photocatalysts are all anatase. The crystallite size is calculated using the Scherrer's equation Tolosa et al. (2011a) and plotted with the adsorption results for gaseous formaldehyde with 2 h runtime as shown in Fig. 5. The crystallite size of the synthesized photocatalysts is about 2–4 times smaller than the other researcher's photocatalysts Hu et al. (2020); Zhang et al. (2017). The adsorption of gaseous formaldehyde follows the same trend as the crystallite size of the synthesized photocatalyst. It is obviously noted that as the crystallite size of the photocatalysts increases, the adsorption also increases. But this contradicts to the theory of the smaller the crystallite sizes the higher the specific surface area leading to higher adsorption capacity.

The specific surface area (SSA), pore size, and pore volume of the commercial Degussa P-25 and synthesized photocatalysts at different calcination time were summarized and presented in Table 2. The results show that the SSA of the synthesized of the titanium dioxide nanoparticles is dependent in the calcination time. It is noted in the result that upon increasing the duration of calcination, the SSA of the synthesized photocatalysts decreases from 175.73 to 171.43 mg^2g^{-1}. This phenomenon will obviously to happen due to sintering process during the calcinations Tolosa et al. (2011a). Prolonged calcination will probably decrease its specific

Table 2
Specific surface area (SSA), pore size and pore volume determination of synthesized photocatalysts using BET.

Photocatalyst	BET surface area (m^2g^{-1})	Single point surface area (m^2g^{-1})	Average pore size (nm)	Pore volume (m^3g^{-1})
C_{y34}	175.73	169.01	4.74	0.21
C_{y35}	174.19	168.89	9.35	0.41
C_{y36}	171.43	165.71	9.41	0.40

surface area due to the presence of unreacted alkoxyl groups during the synthesis and calcination De Luna et al. (2018). This will also confirm that the calcination time affects the specific surface area of the photocatalysts as sown in Table 2.

Comparing the SSA of the three synthesized photocatalysts calcined at 300 °C with different calcination time, with other photocatalysts synthesized by other researcher as discussed previously by Laciste et al. (2017), it shows that the SSA of the photocatalysts of other researcher is 2–4 times lower than the synthesized photocatalysts. The classification of the total porosity of the photocatalyst will be categorized according to their average pore size. As recommended by the IUPAC, the macropores, mesopores, and micropores has the sizes >50 nm, between 2 and 50 nm, and <2 nm, respectively Laciste et al. (2017). As shown in Table 2, synthesized photocatalysts were mesoporous materials with the average pore size ranging from 4.74 to 9.41 nm. The result is significant to the SSA from which the average pore size of the photocatalysts decreases with the increasing SSA. Based on Table 2 result data, it shows that the pore size is between the 2–50 nm which means the synthesized photocatalysts are mesoporous materials. The average pore size is affected by the calcination time wherein upon increasing the time of calcination, the average pore size increases. This occurrence can be attributed to the blocking of the pores of the TiO_2 by the dopant and the sintering during the crystal growth which happens on prolonged calcination.

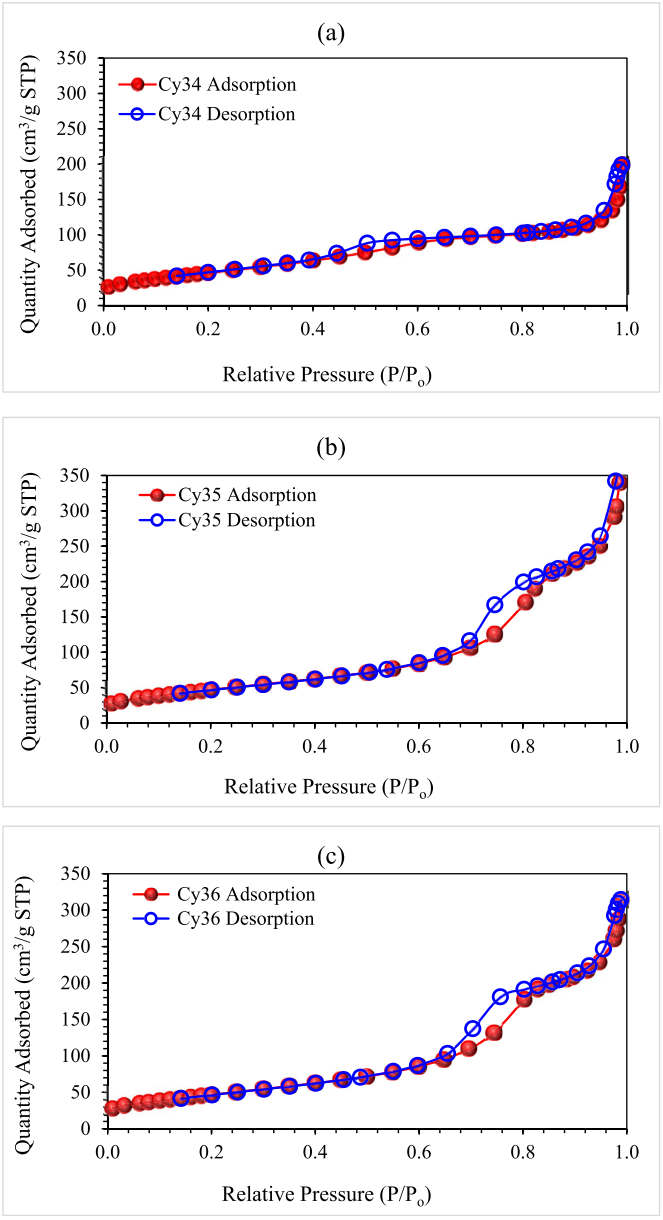

Fig. 6. Nitrogen gas adsorption isotherm plots of multi-elemental doped titanium dioxide nanoparticles calcined at different calcination time.

Fig. 6 shows the nitrogen gas adsorption isotherm plots of three multi-elemental doped titanium dioxide nanoparticles (C_{y34}, C_{y36}, C_{y35}) calcined at different calcination time. The types of pores of the photocatalyst can be identified by the sorption of N_2 gas using the size and shape of their hysteresis loop as shown in Fig. 6. The photocatalyst samples are classified as Type IV with H2 hysteresis loop according to the Brunauer-Deming-Deming-Teller (BDDT) classification that is similar to what another researcher produced Hu et al. (2020); Liu and Lin (2019); Yu et al. (2018); Zhang et al. (2017). The demonstration of the narrow hysteresis loop for all photocatalysts reveals that there is a narrow distribution of cylindrical or tubular pores. The presence of this hysteresis can be correlated to the behavior of the photocatalyst's adsorption capacity through its complicated and interconnected pore network Laciste et al. (2017); Anovitz and Cole (2015). The plots for N_2 gas adsorption isotherms confirm the presence of mesoporous materials and a capillary condensation due to the increased number of van der Waals interaction of the gas molecules De Luna et al. (2018). In Fig. 6, H2 hysteresis is observed for three photocatalysts (C_{y34}, C_{y36}, C_{y35}) which indicates an irregular cylindrical or tubular – shaped pores with narrow opening that can be seen in the higher relative pressure within the plateau region of the hysteresis loop. However, the presence of the narrow hysteresis loop at the plateau region of the lower relative pressure, indicates that there is formation of typical slit-shaped pores of the aggregates of photocatalysts De Luna et al. (2018); Anovitz and Cole (2015).

3.2. Effect of photocatalyst concentration

In this experiment, the effect of the photocatalyst concentration is investigated using different amount of C_{y35} synthesized photocatalyst immobilized on glass tubular reactors, as shown in Fig. 7a, photocatalytic degradation of gaseous formaldehyde increases from 68.7% to 88.1% as the concentration of photocatalyst increased from 0.05 gL^{-1} to 0.10 gL^{-1}. However, the degradation decreases to 83.6% as the photocatalyst dosage increased further to 0.15 gL^{-1}. The increase in the amount of formaldehyde degradation is obviously anticipated since the number of active sites increases with escalating photocatalyst amount. However, the surface area of the

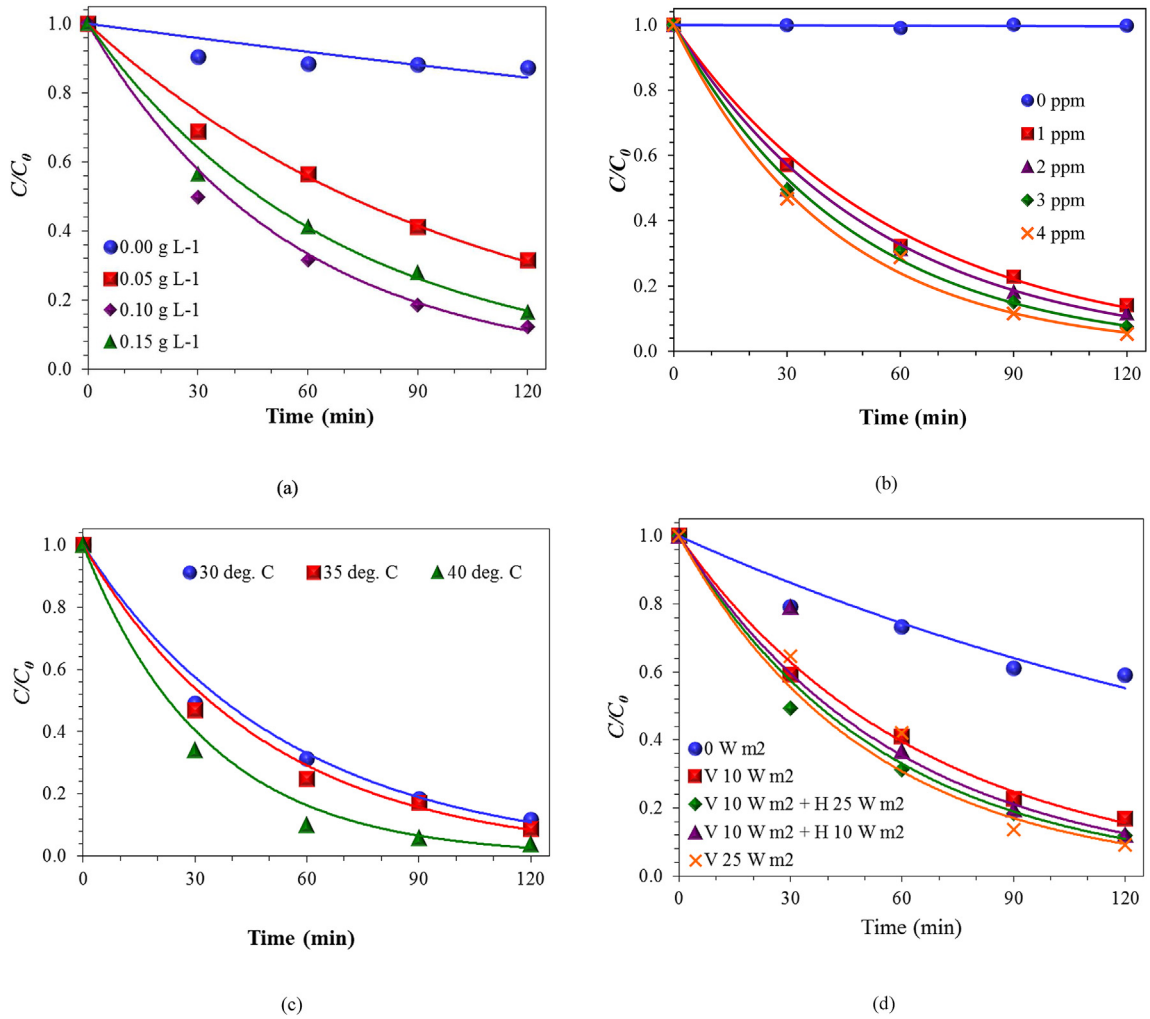

Fig. 7. Residual formaldehyde plot at different (a) photocatalyst loading rate [4 ppm formaldehyde; 30 °C; Vertical 10 Wm^{-2}/Horizontal 25 Wm^{-2}], (b) initial formaldehyde concentration [0.10 gL^{-1}; 30 °C; Vertical 10 Wm^{-2}/Horizontal 25 Wm^{-2}], (c) reaction temperature [0.10 gL^{-1}; 4 ppm formaldehyde; Vertical 10 Wm^{-2}/Horizontal 25 Wm^{-2}], (d) light intensity [0.10 gL^{-1}; 4 ppm formaldehyde; 30 °C].

immobilized photocatalyst is still constant inside the tubes, even though the same vortex speed was used during immobilization. An increase in the amount of immobilized photocatalyst makes the system thicker, as a result the effective light penetration decreases. This is similar to the findings of Muneer et al. (2002) wherein the photocatalyst has an optimum concentration for effective photodegradation. The decrease in degradation is due to the decrease in the amount of photons (light) that penetrated in the system Muneer et al. (2002). On the other hand, there is a slight decrease in formaldehyde concentration in the experiment without catalyst. This is to see the effect of other factors that might contribute to the decrease in formaldehyde concentration. Possible reason should be the effect of the illumination where some of the formaldehyde are destructed by the light. This phenomenon can be correlated to the result in Fig. 7d, where there's a huge decrease in formaldehyde concentration. There was different possibility that affects the huge decrease in formaldehyde concentration. One should be the adsorption of the formaldehyde in catalyst that can be seen also in Fig. 1.

The results show that the photocatalyst concentration with the highest formaldehyde degradation rate is equal to 0.10 gL^{-1}. It is noted that the total formaldehyde removal of about 88.1% after 2 h of illumination. The experimental conditions used in the study are 2 ppm initial formaldehyde concentration, 30 ± 2 °C operating temperature and vertical (V) 10 Wm^{-2}, horizontal (H) 25 Wm^{-2} light orientation.

The photocatalytic degradation of the gaseous formaldehyde follows first-order reaction with the optimum photocatalyst loading. A linear relationship between $-ln(C/C_o)$ versus illumination time, t is observed. Linearized plots of $-ln(C/C_o)$ versus the reaction time using varying photocatalyst dosage are presented in Fig. 8a. The slope of the plot represents the pseudo-first order apparent rate constant, K'. Table 3 shows the apparent rate constants and linearity coefficients, R^2 for the different photocatalyst concentrations used. Pseudo-second order relationship is also examined using linearized plots of $(1/C_o) - (1/C)$ versus time. This is to test which of the rate between the first and second order rate kinetics does the reaction follows in addition to Langmuir-Hinshelwood model. Linearity coefficients for the pseudo-second order relationship are also shown in the table to illustrate the fitness of the system against the pseudo-first order form of the Langmuir-Hinshelwood model. Table 3 shows that the

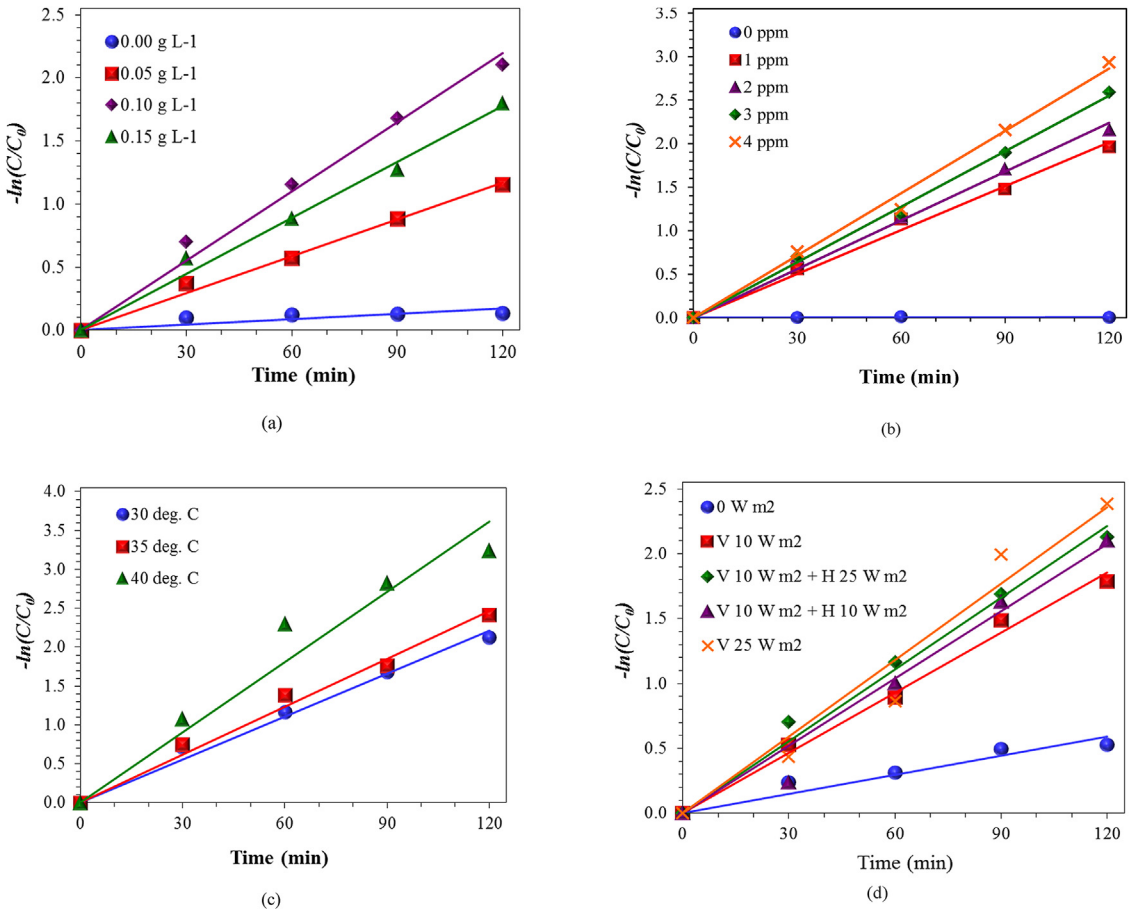

Fig. 8. Linearized plots of ln(C/C$_o$) versus time at different (a) photocatalyst loading rate [4 ppm formaldehyde; 30 °C; Vertical 10 Wm^{-2}/Horizontal 25 Wm^{-2}], (b) initial formaldehyde concentration [0.10 gL^{-1}; 30 °C; Vertical 10 Wm^{-2}/Horizontal 25 Wm^{-2}], (c) reaction temperature [0.10 gL^{-1}; 4 ppm formaldehyde; Vertical 10 Wm^{-2}/Horizontal 25 Wm^{-2}], (d) light intensity [0.10 gL^{-1}; 4 ppm formaldehyde; 30 °C].

Table 3
Apparent pseudo-first order rate constants and pseudo-first and pseudo-second order linearity coefficients using different photocatalyst concentrations for the photocatalytic degradation of gaseous formaldehyde.

Photocatalyst concentration (g/L)	Apparent rate constant, *K'* (Pseudo-First order)	Linearity coefficient, R^2 (Pseudo-first order)	Linearity coefficient, R^2 (Pseudo-second order)
0.05	0.009	0.991	0.877
0.10	0.018	0.987	0.921
0.15	0.014	0.990	0.872

Table 4
Apparent pseudo-first order rate constants and pseudo-first and pseudo-second order linearity coefficients at different initial formaldehyde concentration for the photocatalytic degradation of gaseous formaldehyde.

Initial formaldehyde concentration (ppm)	Apparent rate constant, *K'* (Pseudo-First order)	Linearity coefficient, R^2 (Pseudo-first order)	Linearity coefficient, R^2 (Pseudo-second order)
1	0.016	0.989	0.937
2	0.018	0.987	0.921
3	0.021	0.996	0.829
4	0.023	0.992	0.896

experimental data fitted most to the pseudo-first order kinetics model for gaseous formaldehyde. It can be observed in the result that there was almost no significant change in the pseudo-first order rate constant of different photocatalyst's concentration. This means increasing the immobilized photocatalyst in the borosilicate glass reactor will lead to increasing its thickness without increasing the number of photo-induced photocatalyst particles Jawad et al. (2016). This observation is common to the degradation of the aqueous and volatile organic compounds such as the gaseous formaldehyde.

3.3. Effect of formaldehyde concentration

The effect of the photocatalytic degradation of different initial

Table 5
Apparent pseudo-first order rate constants and pseudo-first and pseudo-second order linearity coefficients at different operating temperatures for the photocatalytic degradation of gaseous formaldehyde.

Operating temperature (°C)	Apparent rate constant, *K'* (Pseudo-First order)	Linearity coefficient, R^2 (Pseudo-first order)	Linearity coefficient, R^2 (Pseudo-second order)
30	0.018	0.987	0.921
35	0.020	0.984	0.896
40	0.029	0.939	0.812

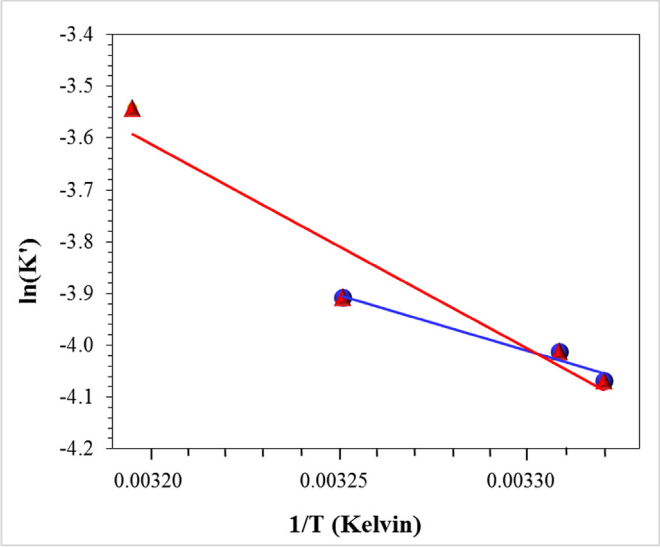

Fig. 9. Arrhenius plot at varying operating temperatures.

formaldehyde concentration (i.e. 0 ppm, 1 ppm, 2 ppm, 3 ppm and 4 ppm) is shown in Fig. 7b. The plot shows almost no significant difference on the residual gaseous formaldehyde with different initial concentrations over illumination time. However, it is noted that this figure indicates that the rate of degradation of gaseous formaldehyde increases with increasing initial concentration. This phenomenon may associated with the reason that at higher initial concentration of gaseous formaldehyde optimized the adsorption in the photocatalyst surface, therefore maximizes its degradation.

In gas phase photocatalysis, the possibility for the gas molecule to reach the photocatalyst surface is dependent on the amount of gas molecules available in the system. It will be more difficult for low concentration formaldehyde to be degraded compared with a higher concentration system. Such that after 2 h illumination, the highest degradation of formaldehyde is at the system of 4 ppm initial concentration with 94% degradation while lowest for the system of 1 ppm initial concentration with 86% degradation.

The photocatalytic degradation reaction follows a first-order reaction from an initial formaldehyde concentration of 1–4 ppm. This is illustrated in the linear relationship of $ln(C/C_o)$ versus illumination time as shown in Fig. 8. Linearized plots of different initial formaldehyde concentrations shown in Fig. 8b fits with the pseudo-first order that gives a straight line. The slope of the pseudo-first order plot gives an apparent first order rate constant *K'*. The apparent rate constants, *K'* and linearity coefficients, R^2 of different initial formaldehyde concentrations are illustrated in Table 4. Linearity coefficients using linearized plots of $(1/C_o) - (1/C)$ versus time are also shown in the table. This is to compare which order of the reaction does this system is best fitted using the pseudo-first order and pseudo-second order form of Langmuir – Hinshelwood model.

3.4. Effect of operating temperature

The gaseous formaldehyde degradation rate as a function of temperature is also examined using synthesized TiO_2 photocatalyst immobilized on glass tubular reactors. Other operating conditions are held constant such as the initial formaldehyde concentration and light orientation system of 2 ppm and V 10 Wm^{-2}, H 25 Wm^{-2}.

In gaseous photocatalysis, the temperature of the reaction should be controlled to ensure the stability of the system in the optimization. In the preliminary experimental data, the system that has a temperature of 50 °C is not stable. Thus, the maximum operating temperature used in this investigation is 40 °C. Fig. 7c presents the effect of varying operating temperatures on the photocatalytic degradation of gaseous formaldehyde. The results show that the gaseous formaldehyde degradation increases with increasing temperatures.

In the experimental study, the operating temperatures of 30 °C, 35 °C, and 40 °C has significance in the photocatalytic degradation of formaldehyde which increased from 88.1, 91.1, and 96.0%, respectively. As compared with the photocatalysis of an aqueous chlorophenols using the same operating temperature range, the photocatalytic degradation does not significantly affected by the operating temperature Tolosa et al. (2011b). This is because the collision frequency of the molecules in gas phase is higher than in the liquid phase even with a small operating temperature increase. This is obvious in the result of the present gaseous photocatalytic study as shown in Fig. 7c wherein reaction temperature considerably affects the photodegradation reaction.

Table 6
Apparent pseudo-first order rate constants and pseudo-first and pseudo-second order linearity coefficients at different light intensities for the photocatalytic degradation of gaseous formaldehyde.

Light intensity (W/m^2)	Apparent rate constant, *K'* (Pseudo-First order)	Linearity coefficient, R^2 (Pseudo-first order)	Linearity coefficient, R^2 (Pseudo-second order)
0 (dark)	0.005	0.919	0.805
10 (vertical)	0.015	0.990	0.934
25 (horizontal)	0.019	0.957	0.830
10 (vertical) 25 (horizontal)	0.018	0.987	0.921
10 (vertical) 10 (horizontal)	0.017	0.972	0.875

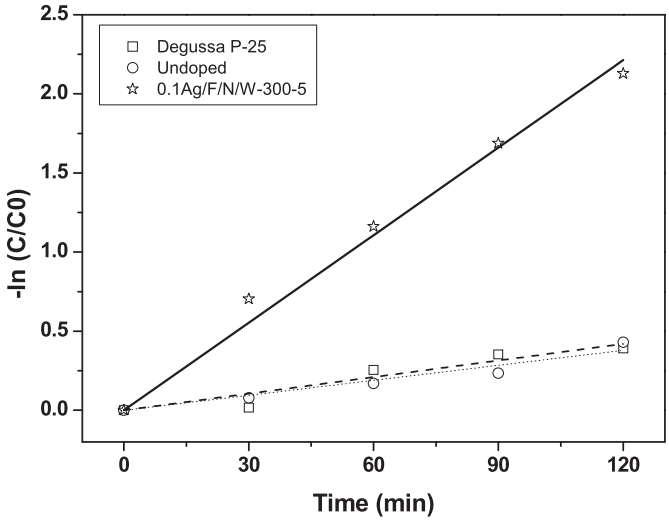

Fig. 10. Formaldehyde degradation rates of the synthesized photocatalyst 0.1 Ag/F/N/W-300-5 (C_{y35}) compared with Degussa P-25 and the unmodified Undoped titanium dioxide calcined at the same condition. 2 ppm formaldehyde, 30 ^{0}C, V 10 Wm^{-2}, H 25 Wm^{-2}.

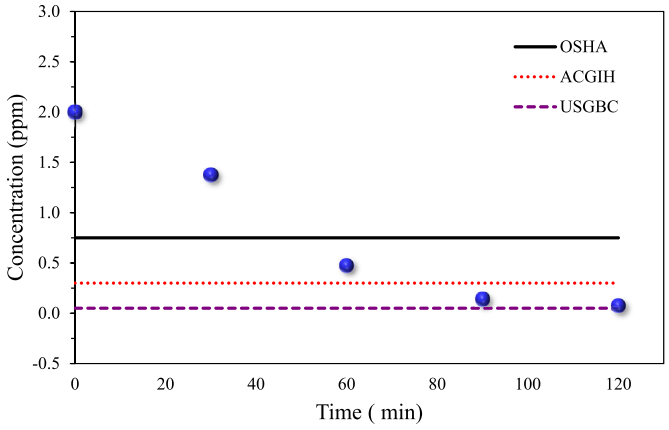

Fig. 11. Formaldehyde degradation plot compared with different guideline values for indoor formaldehyde. Experimental Conditions: 0.1 gL^{-1}of C_{y35}; 3 ppm formaldehyde; 40 °C.

Table 7
Apparent pseudo-first order rate constants and linearity coefficients of pure (undoped) titanium dioxide (U_{35}), Degussa P-25 and C_{y35} photocatalysts.

Photocatalyst	Apparent rate constant, K' (Pseudo-First order)	Linearity coefficient, R^2 (Pseudo-first order)
Degussa P-25	0.003	0.911
U_{35}	0.005	0.966
C_{y35}	0.018	0.987

The photocatalytic degradation of gaseous formaldehyde follows a pseudo-first order expression within the operating temperatures. Linear plots of $-ln(C/Co)$ versus reaction time conducted at different operating temperatures is illustrated Fig. 8c. The apparent rate constants, K' and linearity coefficients, R^2 of the different operating temperatures are shown in Table 5. Linearity coefficients using pseudo-second order rate equation linearized plots of $(1/C_o) - (1/C)$ versus time are also shown in the table to compare from which of the order of reaction in the system best fitted in Langmuir-Hinshelwood model.

Arrhenius' equation as shown in Equation (5) gives the dependence of the rate constant k of a chemical reaction on the absolute temperature T (in Kelvin),

$$k = Ae^{-E_a/RT} \tag{8}$$

where A is the pre-exponential factor, E_a is the activation energy, and R is the universal gas constant.

Taking the natural logarithm of the Arrhenius' equation yields

$$ln\,(K') = -\frac{E_a}{R}\frac{1}{T} + ln\,(A) \tag{9}$$

Thus, when a reaction obeys the Arrhenius equation, a plot of $ln\,(K')$ versus $1/T$ gives a straight line, whose slope and intercept equals $(-E_a/R)$ and A, respectively. Fig. 9 shows the Arrhenius plot of $ln\,(K')$ versus $1/T$. Additional experimental data at 29 °C (K' = 0.17) is included to elucidate the activation energy of the photodegradation of gaseous formaldehyde. Based on the Arrhenius plot in Fig. 9 with the operating temperature range from 29 °C to 40 °C, the activation energy of gaseous formaldehyde degradation is 35.7 kJmol^{-1}. However, upon exclusion of the results from 40 °C, the activation energy is decreased to 19.4 kJmol^{-1}. The linearity coefficient of the latter range is higher (R^2 = 0.962) compared with the former (R^2 = 0.923). It is thus inferred that the activation energy for the degradation of gaseous formaldehyde is 19.4 kJmol^{-1}. This is quite comparable with the value of 20.2 kJmol^{-1} obtained in

Table 8
Apparent pseudo-first order rate constants and linearity coefficients of the synthesized pure (undoped) titanium dioxide, Degussa P-25 and C_{y35} photocatalysts.

Photocatalyst	Loading (g/L)	Formaldehyde concentration (ppm)	Light intensity (W/m^2)		Temperature (°C)	K_{app}	R^2
			V	H			
C_{y35}	0.05	2	10	25	30	0.009	0.991
C_{y35}	0.10	2	10	25	30	0.018	0.987
C_{y35}	0.15	2	10	25	30	0.014	0.990
C_{y35}	0.10	1	10	25	30	0.016	0.989
C_{y35}	0.10	3	10	25	30	0.021	0.996
C_{y35}	0.10	4	10	25	30	0.023	0.992
C_{y35}	0.10	2	10	25	35	0.020	0.984
C_{y35}	0.10	2	10	25	40	0.029	0.939
C_{y35}	0.10	2	0	0	30	0.005	0.919
C_{y35}	0.10	2	10	0	30	0.015	0.990
C_{y35}	0.10	2	0	25	30	0.019	0.957
C_{y35}	0.10	2	10	10	30	0.017	0.972
Degussa-P25	0.10	2	10	25	30	0.005	0.966
U_{35}	0.10	2	10	25	30	0.003	0.911

photocatalytic oxidation of formaldehyde vapor on amorphous titanium dioxide Nikolenko and Melnykov (2010).

In a gaseous system, the collision between the formaldehyde molecules and the photocatalyst will determine the photocatalytic rate. As the operating temperature is increased, the formaldehyde molecules become more dispersed in the system increasing the rate of collision/adsorption of the formaldehyde molecules with the photocatalyst, hence increases the photocatalytic degradation Tolosa et al. (2011b).

3.5. Effect of light intensity

The effect of light intensity was conducted using the orientation of the light source illustrated in Fig. 7d assigned as the vertical light source. The distance of the light source to the tube is varied and light intensity measurements were performed using a Lux meter. As shown in Fig. 7d, the effect of the vertical light source is more pronounced. As the intensity of the vertical light is increased from 10 Wm^{-2} to 25 Wm^{-2}, the degradation increased from 83% to 91%. In contrast, the degradation using the horizontal light source increased from 87.7% to 88.1% only for the intensity of 10 Wm^{-2} to 25 Wm^{-2}. This result is due to the amount of photocatalyst area exposed to the vertical light source compared with the horizontal light source. The amount of photocatalyst activated by the large amount of area exposed to light is larger using the vertical light source compared with the horizontal light source orientation.

Linearized plots of $-ln(C/C_o)$ versus reaction time at different light intensities is shown in Fig. 8d. The apparent rate constants, K' and linearity coefficients, R^2 of the different light intensities are shown in Table 6. Linearity coefficients using linearized plots of $(1/C_o) - (1/C)$ versus time are also shown in the table to show that the system is best fitted using the pseudo-first order form of Langmuir-Hinshelwood model.

3.6. Performance comparison of commercial (Degussa P-25) and undoped TiO_2

The performance of the modified catalyst was evaluated and compared with a commercial Degussa P-25 and undoped photocatalyst to show the effect of the modifications applied. Fig. 10 shows the difference of the synthesized photocatalyst over Degussa P-25 and undoped photocatalyst in the degradation of the gaseous formaldehyde. Using an optimized condition of 0.10 gL^{-1} dosage, 30 °C operating temperature, and 4 ppm initial formaldehyde concentration, C_{y35} shows superiority in photocatalytic degradation as compared with Degussa P-25 and undoped titanium dioxide with the difference of 55.8% and 37.7%, respectively.

The apparent pseudo-first order rate constants and linearity coefficients of the synthesized photocatalyst, commercial Degussa P-25 and undoped titanium dioxide are shown in Table 7 and Fig. 10. The results show that the photocatalytic oxidation of the gaseous formaldehyde with the synthesized photocatalysts (C_{y35}) is about 3.6 and 6 times faster than the undoped and Degussa P-25, respectively. This means that C_{y35} is excellent in oxidizing volatile organic compounds such as gaseous formaldehyde. In summary, Table 8 lists the apparent rate constant of the synthesized photocatalyst, C_{y35} at varying kinetic conditions. The apparent rate constant for Degussa P-25 and the undoped synthesized photocatalyst is also included.

3.7. Compliance with the guideline values

Indoor formaldehyde guideline values are used as standard in evaluating the residual formaldehyde concentration in photocatalysis to verify the synthesized photocatalyst for its performances. The published formaldehyde exposure limits in 2008 are administered by the following, the Occupational Safety and Health Administration (OSHA) Permissible Exposure Limit (PEL) = 0.75 ppm, American Conference of Government Industrial Hygienists (ACGIH) Ceiling Concentration (C) = 0.3, and United States Green Buildings Council (USGBC) Leadership in Energy and Environmental Design (LEED) limit = 0.05. As shown in Fig. 11, the synthesized photocatalyst (C_{y35}) using the following experimental conditions: 120 min runtime, 40 °C operating temperature, 3 ppm initial formaldehyde concentration and 0.1 gL^{-1} photocatalyst concentration can degrade gaseous formaldehyde and comply within the standards of 60, 90 and 120 min for OSHA PEL standards, ACGIH C limit and USGBC LEED standard, respectively.

4. Conclusion

Synthesized photocatalyst was modified and investigated at varying calcination time of 4, 5, and 6 h. The photodegradation of formaldehyde increases as calcination time increased to 5 h with about 88%. The kinetics of gaseous formaldehyde through photocatalytic degradation is examined by varying the photocatalyst concentration, pollutant concentration, operating temperature and light intensity. The optimum photocatalyst concentration is observed at 0.1 gL^{-1} and related to the amount of light that can penetrate the system. Furthermore, increasing the photocatalyst concentration resulted to an observable decrease in degradation rate. The photocatalyst degradation rate increased when the initial formaldehyde concentration is varied from 0 ppm to 4 ppm. Increasing the operational temperatures from 30 °C to 40 °C resulted to an increase in photocatalytic degradation rates. The activation energy of gaseous formaldehyde from photocatalytic degradation is 19.4 $kJmol^{-1}$. This is comparable to similar studies on gaseous formaldehyde photocatalysis. The light intensity and orientation resulting to higher degradation are 25 Wm^{-2} and vertical configuration wherein the maximum photocatalyst area is exposed.

The photocatalytic degradation behavior of gaseous formaldehyde of the modified photocatalyst follows a pseudo-first order rate equation based on a Langmuir-Hinshelwood kinetic type of model. The C_{y35} photocatalyst has the superiority on the photocatalytic performance compared with the undoped $TiO_2$and commercial Degussa P-25 by 37.7% and 55.8% by difference, respectively. Based on the set experimental conditions, the synthesized photocatalyst can comply with OSHA, ACGIH, and USGBC standards within the 2-h illumination time.

Author's contributions

MCL and MDGDL conceptualized the research work and supervised the completion of each task in the study. MTL, MDGDL and NCT reviewed the literature on the topic. MTL designed the reactor. MDGDL designed the experiments. MTL synthesized and characterized the catalysts. MTL performed the formaldehyde degradation experiments. NCT, MTL and MDGDL analyzed the results. MTL, MDGDL and NCT organized the results and wrote the draft of the manuscript. All authors revised and approved the final manuscript.

Declaration of interest statement

The authors declare that they have NO pecuniary or other personal interest, direct or indirect, in any matter that raises or may raise a conflict with our obligations as authors in this manuscript. The funders had no role in the design of the study; in the collection, analyses, or interpretation of data; in the writing of the manuscript, and in the decision to publish the results.

Acknowledgments

The authors are grateful to the National Science Council, Taiwan (NSC 101-2923-E-041-001-MY2) and the Department of Science and Technology, Philippines for funding this research.

References

Anovitz, L.M., Cole, D.R., 2015. Characterization and analysis of porosity and pore structures. Rev. Mineral. Geochem. 80, 61–164.

Cheng, Z.W., Feng, L., Chen, J.M., Yu, J.M., Jiang, Y.F., 2013. Photocatalytic conversion of gaseous ethylbenzene on lanthanum-doped titanium dioxide nanotubes. J. Hazard Mater. 254–255, 354–363. https://doi.org/10.1016/j.jhazmat.2013.03.037.

De Luna, M.D.G., Laciste, M.T., Tolosa, N.C., Lu, M.C., 2018. Effect of catalyst calcination temperature in the visible light photocatalytic oxidation of gaseous formaldehyde by multi-element doped titanium dioxide. Environ. Sci. Pollut. Res. 25 (15), 15216–15225. https://doi.org/10.1007/s11356-018-1720-0.

De Luna, M.D.G., Garcia-Segura, S., Mercado, C.H., Lin, Y.-T., Lu, M.-C., 2019. Doping TiO_2 with $CuSO_4$ enhances visible light photocatalytic activity for organic pollutant degradation. Environ. Sci. Pollut. Res. https://doi.org/10.1007/s11356-019-05789-5.

Debono, O., Thévenet, F., Gravejat, P., Héquet, V., Raillard, C., Le Coq, L., Locoge, N., 2013. Gas phase photocatalytic oxidation of decane at ppb levels: removal kinetics, reaction intermediates and carbon mass balance. J. Photochem. Photobiol. A Chem. 258, 17–29. https://doi.org/10.1016/j.jphotochem.2013.02.022.

Fujishima, A., Zhang, X., Tryk, D.A., 2008. TiO_2 photocatalysis and related surface phenomena. Surf. Sci. Rep. 63, 515–582. https://doi.org/10.1016/j.surfrep.2008.10.001.

Haber, J., Nowak, P., Zurek, P., 2008. Charge transfer in photocatalytic systems: V and Mo doped TiO_2/Ti electrodes. Catal. Lett. 43, 48. https://doi.org/10.1007/s10562-008-9652-9.

Han, Z., Chang, V.W., Wang, X., Lim, T.T., Hildemann, L., 2013. Experimental study on visible-light induced photocatalytic oxidation of gaseous formaldehyde by polyester fiber supported photocatalysts. Chem. Eng. J. 218, 9–18. https://doi.org/10.1016/j.cej.2012.12.025.

Harb, P., Locoge, N., Thevenet, F., 2020. Treatment of household product emissions in indoor air: real scale assessment of the removal processes. Chem. Eng. J. 380, 122525 https://doi.org/10.1016/j.cej.2019.122525.

He, Z., Hong, T., Chen, J., Song, S., 2012. A magnetic TiO_2 photocatalyst doped with iodine for organic pollutant degradation. Separ. Purif. Technol. 96, 50–57. https://doi.org/10.1016/j.seppur.2012.05.005.

Hu, X., Li, C., Sun, Z., Song, J., Zheng, S., 2020. Enhanced photocatalytic removal of indoor formaldehyde by ternary heterogeneous BiOCl/TiO_2/sepiolite composite under solar and visible light. Build. Environ. 168 https://doi.org/10.1016/j.buildenv.2019.106481, 106481.

Jawad, A.H., Mubarak, N.S.A., Ishak, M.A.M., Ismail, K., Nawawi, W.I., 2016. Kinetics of photocatalytic decolourization of cationic dye using porous TiO_2 film. J. Taibah U. Sci. 10, 352–362.

Jin, M., Zhang, X., Pu, H., Nishimoto, S., Taketoshi, M., 2011. Photochromism-based detection of volatile organic compounds by W-doped TiO_2 nanofibers. J. Colloid Interface Sci. 362, 188–193. https://doi.org/10.1016/j.jcis.2011.06.041.

Laciste, M.T., de Luna, M.D.G., Tolosa, N.C., Lu, M.C., 2017. Degradation of gaseous formaldehyde via visible light photocatalysis using multi-element doped Titania nanoparticles. Chemosphere 182, 174–182. https://doi.org/10.1016/j.chemosphere.2017.05.022.

Lai, H.K., Jantunen, M.J., Künzli, N., Kulinskaya, E., Colvile, R., Nieuwenhuijsen, M.J., 2007. Determinants of indoor benzene in Europe. Atmos. Environ. 41 (39), 9128–9135. https://doi.org/10.1016/j.atmosenv.2007.08.001.

Li, Y., Jiang, Y., Peng, S., Jiang, F., 2010. Nitrogen-doped TiO_2 modified with NH_4F for efficient photocatalytic degradation of formaldehyde under blue light-emitting diodes. J. Hazard Mater. 182 (1 – 3), 90–96. https://doi.org/10.1016/j.jhazmat.2010.06.002.

Lin, J.C.-T., De Luna, M.D.G., Aranzamendez, G.L., Lu, M.-C., 2016. Degradations of acetaminophen via a $K_2S_2O_8$-doped TiO_2 photocatalysts under visible light irradiation. Chemosphere 155, 388–394. http://doi.org/10.1016/j.chemosphere.2016.04.059.

Liu, S.-H., Lin, W.-X., 2019. A simple method to prepare g-C_3N_4-TiO_2/waste zeolites as visible-light-responsive photocatalytic coatings for degradation of indoor formaldehyde. J. Hazard Mater. https://doi.org/10.1016/j.jhazmat.2019.01.082.

Liu, H., Lian, Z., Ye, X., Shangguan, W., 2005. Kinetic analysis of photocatalytic oxidation of gas-phase formaldehyde over titanium dioxide. Chemosphere 60, 630–635. https://doi.org/10.1016/j.chemosphere.2005.01.039.

Liu, T., Li, F., Li, X., 2008. TiO_2 hydrosols with high activity for photocatalytic degradation of formaldehyde in a gaseous phase. J. Hazard Mater. 152 (1), 347–355. https://doi.org/10.1016/j.jhazmat.2007.07.003.

Muneer, M., Singh, H.K., Bahnemann, D.W., 2002. Semiconductor mediated photocatalyzed degradation of two selected priority organic pollutants, benxidine and 1,2-diphenylhydrazine in aqueous suspension. Chemosphere 49, 193–203. https://doi.org/10.1016/S0045-6535(02)00190-X.

Nikolenko, A., Melnykov, B., 2010. Photocatalytic oxidation of formaldehyde vapour using amorphous titanium dioxide. Chem. Chem. Technol. 4 (4), 311–315.

Pei, J., Yin, Y., Liu, J., Dai, X., 2020. An eight – city study of volatile organic compounds in Chinese residences: compounds, concentrations and characteristics. Sci. Total Environ. 698 https://doi.org/10.1016/j.scitotenv.2019.134137, 134137.

Putta, T., Lu, M.C., Anotai, J., 2011. Photocatalytic activity of tungsten-doped TiO_2 with hydrothermal treatment under blue light irradiation. J. Environ. Manag. 92, 2272–2276. https://doi.org/10.1016/j.jenvman.2011.04.016.

Rezaee, A., Rangkooy, H., Jonidi-Jafari, A., Khavanin, A., 2013. Surface modification of bone char for removal of formaldehyde from air. Appl. Surf. Sci. 286, 235–239. https://doi.org/10.1016/j.apsusc.2013.09.053.

Salthammer, T., 2019. Formaldehyde sources, formaldehyde concentrations and air exchange rates in European housings. Build. Environ. 150, 219–232. https://doi.org/10.1016/j.buildenv.2018.12.042.

Sánchez, B., Sánchez-Muñoz, M., Muñoz-Vicente, M., Cobas, G., Portela, R., Suárez, S., González, A.E., Rodríguez, N., Amils, R., 2012. Photocatalytic elimination of indoor air biological and chemical pollution in realistic conditions. Chemosphere 87 (6), 625–630. https://doi.org/10.1016/j.chemosphere.2012.01.050.

Senthilnanthan, M., Ho, D., Vigneswaran, S., Ngo, H., Shon, H., 2012. Visible light responsive ruthenium-doped titanium dioxide for the removal of metsulfuron-methyl herbicide in an aqueous phase. Separ. Purif. Technol. 415, 419. https://doi.org/10.1016/j.seppur.2010.05.019.

Shie, J.L., Lee, C.H., Chiou, C.S., Chang, C.T., Chang, C.C., Chang, C.Y., 2008. Photodegradation kinetics of formaldehyde using light sources of UVA, UVC and UVLED in the presence of silver titanium oxide photocatalyst. J. Hazard Mater. 155, 164–172. https://doi.org/10.1016/j.jhazmat.2007.11.043.

Sonowane, R.S., Kale, B.B., Dongare, M.K., 2004. Preparation and photo-catalytic activity of Fe-TiO_2 thin films prepared by sol-gel dip coating. Mater. Chem. Phys. 85, 52–57. https://doi.org/10.1016/j.matchemphys.2003.12.007.

Tabaei, H.S., Kazemeini, M., Fattahi, M., 2012. Preparation and characterization of visible light sensitive nano titanium dioxide photocatalyst. Sci. Iran. 19 (6), 1626–1631.

Tolosa, N.C., Lu, M.C., Mendoza, H.D., Rollon, A.P., 2011a. The effect of the composition of tri-elemental doping (K, Al, S) on the photocatalytic performance of synthesized TiO_2 nanoparticles in oxidizing 2-chlorophenol over visible light illumination. Appl. Catal. Gen. 401, 233–238. https://doi.org/10.1016/j.apcata.2011.05.028.

Tolosa, N.C., Lu, M.C., Mendoza, H.D., Rollon, A.P., 2011b. Factors affecting the photocatalytic oxidation of 2,4-dichlorophenol using modified titanium dioxide TiO_2/$KAl(SO_4)_2$ catalyst under visible light. Sustain. Environ. Res. 21 (6), 381–387.

Villaluz, F.J.A., De Luna, M.D.G., Colades, J.I., Garcia-Segura, S., Lu, M.-C., 2019. Removal of 4-chlorophenol by visible-light photocatalysis using ammonium iron (II) sulfate-doped nano-titania. Process Saf. Environ. Prot. https://doi.org/10.1016/j.psep.2019.03.001.

Wang, X., Lim, T.T., 2011. Effect of hexamethylenetetramine on the visible-light photocatalytic activity of C-N co-doped TiO_2 for bisphenol A degradation: evaluation of photocatalytic mechanism and solution toxicity. Appl. Catal. Gen. 399 (1 – 2), 233–241. https://doi.org/10.1016/j.apcata.2011.04.002.

Wilke, K., Breuer, H.D., 1999. The influence of transition metal doping on the physical and photocatalytic properties of Titania. J. Photochem. Photobiol., A 121 (1), 49–53.

Wu, J.C., Chen, C., 2004. A visible-light response vanadium-doped Titania nanocatalyst by sol-gel method. J. Photochem. Photobiol. A Chem. 163, 509–515. https://doi.org/10.1016/j.jphotochem.2004.02.007.

Wu, Y., Hu, X., Xie, T., Li, G., Zhang, L., 2005. Phase structure of W-doped nano-TiO_2 produced by sol-gel method. China Particuol. 3 (4), 233–236.

Xiao, G., Huang, A., Su, H., Tan, T., 2013. The activity of acrylic-silicon/nano-TiO_2 films for the visible-light degradation of formaldehyde and NO_2. Build. Environ. 65, 215–221.

Yu, B.F., Hu, Z.B., Liu, M., Yang, H.L., Kong, Q.X., Liu, Y.H., 2009. Review of research on air-conditioning system and indoor air quality control for human health. Int. J. Refrig. 32 (1), 3–20. https://doi.org/10.1016/j.ijrefrig.2008.05.004.

Yu, L., Wang, L., Sun, X., Ye, D., 2018. Enhanced photocatalytic activity of rGO/TiO_2 for the decomposition of formaldehyde under visible light irradiation. https://doi.org/10.1016/j.jes.2018.01.022.

Zhang, X., Liu, Q., 2008. Visible-light-induced degradation of formaldehyde over Titania photocatalyst co-doped with nitrogen and nickel. Appl. Surf. Sci. 254, 4780–4785. https://doi.org/10.1016/j.apsusc.2008.01.094.

Zhang, G., Sun, Z., Duan, Y., Ma, R., Zheng, S., 2017. Synthesis of nano-TiO_2/diatomite composite and its photocatalytic degradation of gaseous formaldehyde. Appl. Surf. Sci. http://doi.org/10.1016/j.apsusc.2017.03.198.

Zhong, J.B., Lu, Y., Jiang, W.D., Meng, Q.M., He, X.Y., Li, J.Z., Chen, Y.Q., 2009. Characterization and photocatalytic property of Pd/TiO_2 with the oxidation of gaseous benzene. J. Hazard Mater. 168 (2 – 3), 1632–1635. https://doi.org/10.1016/j.jhazmat.2009.02.158.